Available online at www.sciencedirect.com
ScienceDirect
Earth and Planetary Science Letters 260 (2007) 549–563
EPSL
www.elsevier.com/locate/epsl

The crust and upper mantle structure beneath southeastern China

Yinshuang Ai [a,b,*], Qi-fu Chen [c], Fei Zeng [d], Xing Hong [d], Wenyan Ye [d]

[a] *State Key Laboratory of Lithospheric Evolution, Institute of Geology and Geophysics, Chinese Academy of Sciences, Beituchengxilu 19, Chaoyang District, Beijing 100029, China*
[b] *Institute of Tibetan Plateau Research, Chinese Academy of Sciences, Beijing 100085, China*
[c] *Institute of Earthquake Science, China Earthquake Administration, P. O. Box 166, Beijing 100036, China*
[d] *Earthquake Administration of Fujian Province, Fuzhou 350003, China*

Received 15 July 2006; received in revised form 29 May 2007; accepted 2 June 2007
Available online 12 June 2007
Editor: R.D. van der Hilst

Abstract

We analyzed teleseismic waveforms recorded by 44 stations in the Fujian and Taiwan provinces of China and obtained 5344 high quality receiver functions. The crustal thickness (H) and average crustal V_P/V_S ratio (k) beneath every station were estimated using the H–k stacking method. Crustal thicknesses near the Fujian Province range from 28.3 to 32.8 km with an average of 31.1 km, and the corresponding V_P/V_S ratios vary from 1.70 to 1.84 with a mean of 1.76. From inland to offshore of the Fujian Province, the crustal thicknesses decrease and Poisson's ratios increase. These may indicate decreasing SiO_2 and increasing calc-alkaline contents in the crust. The discontinuity structures such as the Moho, subducting slab, the 410- and 660-km discontinuities (hereafter we call them the 410 and the 660) are also studied using common converted point (CCP) stacking of receiver functions. Along two NW–SE lines of central and northern Taiwan, the CCP stacking results show a western dipping structure at depths above 50 km, suggesting that the Philippine Sea plate is probably subducting beneath the Eurasian continent plate near the central and northern Taiwan. The CCP stacking results show sharp and flat 410- and 660-km discontinuities, and the transition zone thickness (TZT) is the same as that of ambient mantle beneath Fujian and Taiwan Strait, but thickens in the east of Taiwan. These results suggest that (1) the subducting Eurasian continent plate is confined to the depths above 410 km beneath Fujian and Taiwan Strait; and (2) the South China Sea slab may reach the transition zone beneath the east of Taiwan.

Keywords: receiver functions; crustal thickness; Poisson's ratio; slab; the upper mantle discontinuity

1. Introduction

Located on the western Pacific margin, southeastern China is an ideal natural laboratory to study modern plate interaction and geodynamics. In this area, the Eurasian and Philippine Sea plates converge in the region of Taiwan. In northeastern Taiwan, the relative plate motion between the Philippine Sea plate and the Eurasian plate is in a NW direction with an estimated rate of 8.2 cm/yr (Yu et al., 1997), whereas in southern Taiwan, the plate motion between the South China plate and the Luzon arc of the Philippine Sea plate is eastward (Kim et al., 2004). As a consequence of plate collision, the Taiwan mountain belt, one of the youngest

* Corresponding author. State Key Laboratory of Lithospheric Evolution, Institute of Geology and Geophysics, Chinese Academy of Sciences, Beituchengxilu 19, Chaoyang District, Beijing 100029, China. Tel.: +86 10 62007354; fax: +86 10 62010846.
E-mail address: ysai@mail.iggcas.ac.cn (Y. Ai).

0012-821X/$ - see front matter © 2007 Elsevier B.V. All rights reserved.
doi:10.1016/j.epsl.2007.06.009

orogenesis in the world, was formed (Sibuet and Hsu, 2004). The nearest continental area to Taiwan is the Fujian Province, China, which is located to the northwest of Taiwan. Late Mesozoic igneous rocks occur over a large area in Fujian due to the combination of lithosphere subduction and underplating of mafic magmas (Zhou and Li, 2000).

In order to demonstrate the collision model between the Philippine Sea plate and the Eurasian plate in southeastern China, particularly in the Taiwan region, many studies have been carried out in the past few decades. Based on the sedimentology and stratigraphy in the Western Foothills of Taiwan, Suppe suggested a thin-skinned deformation model to explain the mountain building in Taiwan (Suppe, 1984). Wu et al. proposed lithospheric collision between the Luzon arc and Eurasian lithosphere (Wu et al., 1997), to interpret the distribution of earthquake hypocenters. To investigate the deep interior structure, global seismic travel-time tomography has been performed in this region (Lallemand et al., 2001). The tomographic results have demonstrated that the Eurasian plate subducts beneath most parts of the Taiwan island down to the bottom of the mantle transition zone and both the Eurasian plate and the Philippine Sea slabs interact beneath northern Taiwan (Lallemand et al., 2001). However, due to sparse data, the global tomographic results cannot reveal the plate interactions in great detail.

Even though many geophysical studies have been performed in southeastern China, there are still many problems to be solved. First, the subduction of the Philippine Sea plate beneath the Eurasian plate produces the Ryukyu subduction zone in northeastern Taiwan. The Ryukyu slab geometry in the northeast has been well determined (Font et al., 1999), but its western termination remains poorly defined. Second, although it is known that the Taiwan orogeny was created by the interaction between the Eurasian plate and Philippine Sea plate, there is uncertainty on how the Eurasian plate was deformed, such as in the Fujian Province. Finally, in order to further understand the detailed interaction between the Eurasian plate and the Philippine Sea plate in southeastern China, it is vital to resolve properties of the deep interior structure in this region. However, besides some tomographic results (Lallemand et al., 2001), very few seismic constraints on the deep structure in this area are available. To better answer the above questions, we used the receiver function technique to study the deep interior structure beneath the southeastern China region.

Due to the increasing number of digital seismic stations and modern data processing methods from exploration seismology, receiver function stacking methods have been widely used to study the interior structure of the Earth in recent years (e.g. Dueker and Sheehan, 1997; Yuan et al., 1997; Zhu and Kanamori, 2000). In this study, we used a large amount of teleseismic events recorded by stations in Taiwan and the Fujian Province. Combining the data from two regions gives a better coverage of the deep structure because their ray-paths cross each other. Furthermore, the detailed crustal and uppermost mantle structures in the two regions can provide more robust evidence for interaction between the Eurasian plate and Philippine Sea plate.

2. Data and methods

2.1. Data

In this study, we utilized seismic waveforms recorded by three local networks, Fujian Seismic Network (FJN), Broadband Array in Taiwan for Seismology (BATS), and New China Digital Seismology Network (NCDSN) (Fig. 1).

FJN was deployed in 1999 by the Earthquake Administration of the Fujian Province. It consists of 9 broadband and 20 short period stations within the Fujian Province. All of them have operated continuously from June 1999 to the present, and record at a rate of 50 samples per second with three components. Because they were deployed in mountainous areas and maintained carefully, the data are of high-quality. Therefore, we selected teleseismic events in the distance range between 30° and 90° with magnitude greater than 5.8 for the receiver functions analysis. The data from FJN used in this study spans the time interval from January 2000 to October 2005.

BATS consists of 13 broadband stations. Eleven are located on the island of Taiwan and two are located offshore of mainland China (Fig. 1). Some stations in BATS operated with three components from the mid 1990s to the present, and recorded continuously at 40 samples per second (Kao et al., 1998). Furthermore, due to site location, noisy environment or technical problems, the BATS data is of lower-quality compared with that of FJN. Thus, we selected teleseismic events from BATS in the same distance range as the FJN data, but of events with magnitudes greater than 6.0 for the receiver functions analysis. Besides the data from BATS, we also downloaded data with magnitudes greater than 6.0 from one GSN (Global Seismograph Network) station in Taiwan, TATO, for which data spanned from January 1995 to November 2005.

The last data set was from NCDSN. In southern China, only one broadband station WZH is located near

the Fujian Province. We selected teleseismic events with the same criterion as the FJN data at this station with data spanned from October 2000 to August 2003.

2.2. Receiver function isolation

Receiver functions for each event-station pair were isolated according to the following. First, we visually checked each event carefully to make sure that the event has a clear first P phase and is high-quality recording. Second, the selected seismograms were cut from 20 s before to 100 s after the first P wave arrivals. Then, a 2.5 Hz Gaussian parameter, which excludes frequencies over about 1.2 Hz (Ammon, 1991), was used to calculate receiver functions by the maximum entropy deconvolution method (Wu and Zeng, 1998; Ai et al., 2003). Finally, we visually selected records with high signal-to-noise ratios for each station to ensure that the *P*-to-*S* converted phase from the Moho and its two later multiple phases are present (Ai et al., 2005). For 30 FJN and NCDSN stations, the number of receiver functions selected varies from 35 at station LIJ to 193 at station CHT. In total, 3315 reliable receiver functions were obtained. For the BATS and GSN stations, the number of receiver functions obtained varies from 0 at station HWAB to 340 at station KMNB, for a total of 2029 useful receiver functions. As a whole, 5344 receiver functions were obtained for all 44 stations in the southern China region. These receiver functions were calculated from 856 teleseismic events, with most events distributed to the south and southeast of the study region (Fig. 2).

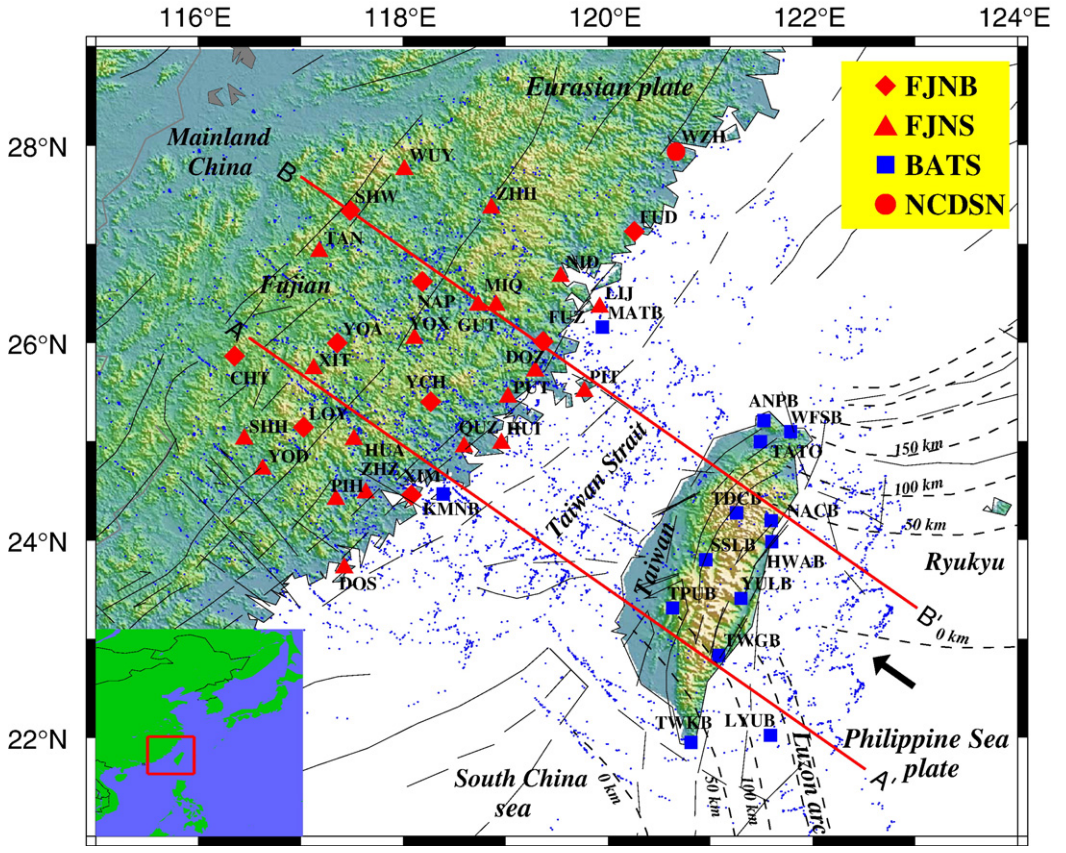

Fig. 1. Map showing the present study region in Southeastern China and the seismic stations used in this study (see also the insert map). Locations of seismic stations are shown by red diamonds for FJNB — Broadband stations of Fujian Network, red triangles for FJNS — Short period stations of Fujian Network, blue squares for BATS — Broadband Array in Taiwan for Seismology, and red circles for NCDSN — New China Digital Seismology Network, respectively. Station codes are shown near stations with three or four capital letters. The vector of relative motion between the Philippine Sea plate and the Eurasian plate is shown by the arrow (Yu et al., 1997). Dashed lines denote the depth contours of the subducting Eurasian plate along Manila Trench and the subducting Philippine Sea plate along Ryukyu Trench, respectively (after Gudmundsson and Sambridge, 1998). Solid lines denote fault locations. Blue dots represent the piercing points of converted S waves at depth of 410 km. The locations of two stacking profiles are shown in AA′, BB′.

2.3. Methods

Receiver function methods have been widely used to study the deep structure of the Earth since they were introduced to seismology about three decades ago (Langston, 1977; Vinnik, 1977). In this study, we used two standard receiver function methods, H–k and CCP stacking techniques (Zhu and Kanamori, 2000; Chevrot and van der Hilst, 2000; Zhu, 2000), to study the interior structure of southern China.

The previous studies have shown that jointly using the converted phase from the Moho and its multiple reverberations within the crust, can give an accurate estimate of the crustal thickness and V_P/V_S ratio (Zandt and Ammon, 1995). However, because of background noise, P-to-S conversions, and its multiples from other velocity discontinuities in the crust, identifying the Moho Ps and its multiples and measuring their arrival times on a receiver function trace can be difficult (Zhu and Kanamori, 2000). Therefore, the auto-searching algorithm, H–k method, which sums the amplitudes of the receiver functions at the predicted arrival times of Ps and its multiple phases, has been developed to determine the best estimations of crustal thickness (H) and V_P/V_S ratio (k), simultaneously (Zhu and Kanamori, 2000; Chevrot and van der Hilst, 2000). When the stacking process was performed, weights were assigned to different converted phases and their multiples.

In this study, we also used the CCP stacking algorithm (Kosarev et al., 1999; Zhu, 2000, 2002), to constrain the lateral variation of crustal and upper mantle discontinuities beneath southeastern China. This standard method includes the following processes (Zhu, 2000, 2002): (1) By using a known background velocity model, the depth domain ray-path of each receiver function is calculated. (2) After correcting for the incidence angle effect, the amplitude at each point on the radial receiver function is assigned to its position on the ray-path where the P-to-S conversion is assumed to occur. (3) The studied profile is divided into bins and all amplitudes in the same bin are stacked to obtain the average amplitude. (4) When the stacking is performed, the width of the ray is calculated using its Fresnel zone size to produce smooth images. The smoothing distance

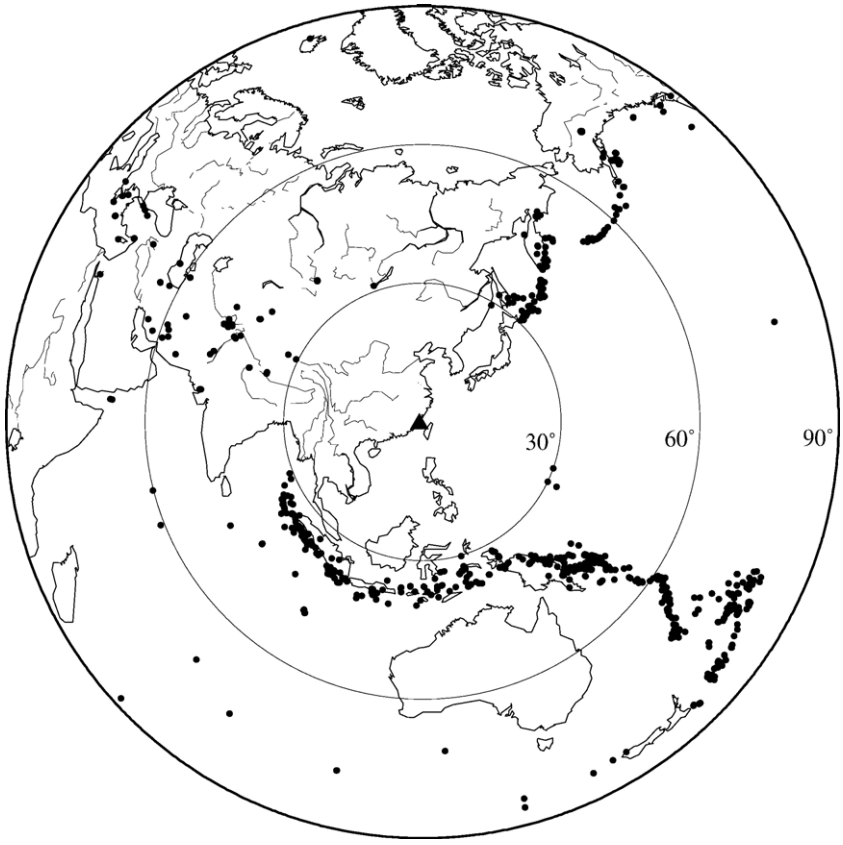

Fig. 2. Epicenter distribution of teleseismic events used in this study. Most events are distributed on the south, southeast, northeast, and northwest of the study region. The map center (black triangle) is (119.77° E, 25.50° N).

varies adaptively according to the size of the Fresnel zone at different stacking depths.

3. Crustal thickness and Poisson's ratio

There are several key parameters which need to be specified in advance when using the H–k stacking method. The first one is the average crustal P velocity (Zhu and Kanamori, 2000; Chevrot and van der Hilst, 2000). Previous studies have shown that the average crustal P velocities for Fujian and Taiwan are similar (Kim et al., 2004; Chen et al., 2005). Chen et al. (2005) integrated many geophysical data in southeastern China and obtained an average crustal P velocity of 6.3 km/s. In this study, we used this value as prior parameter. Second, the ranges of crustal thickness and V_P/V_S ratio for each station need to be given. Previous studies show that crustal thicknesses vary from 29 to 32 km in the Fujian Province, however, they vary greatly from 28 to 52 km in Taiwan (Kim et al., 2004; Chen et al., 2005). In H–k stacking, the crustal thicknesses were constrained, from 27 to 40 km for FJN and NCDSN stations, and 20 to 55 km for BATS and GSN stations, respectively. For V_P/V_S ratio, the value was limited between 1.6 and 2.0. Third, weights for the P-to-S converted phase from the Moho and its later multiples need to be assigned. The highest weight was assigned to the P-to-S converted phase from the Moho, because it has the highest signal-to-noise ratio. The values ultimately used were 0.7 for the P-to-S converted phase from Moho, 0.2 for PpPs, and 0.1 for PpSs+PsPs.

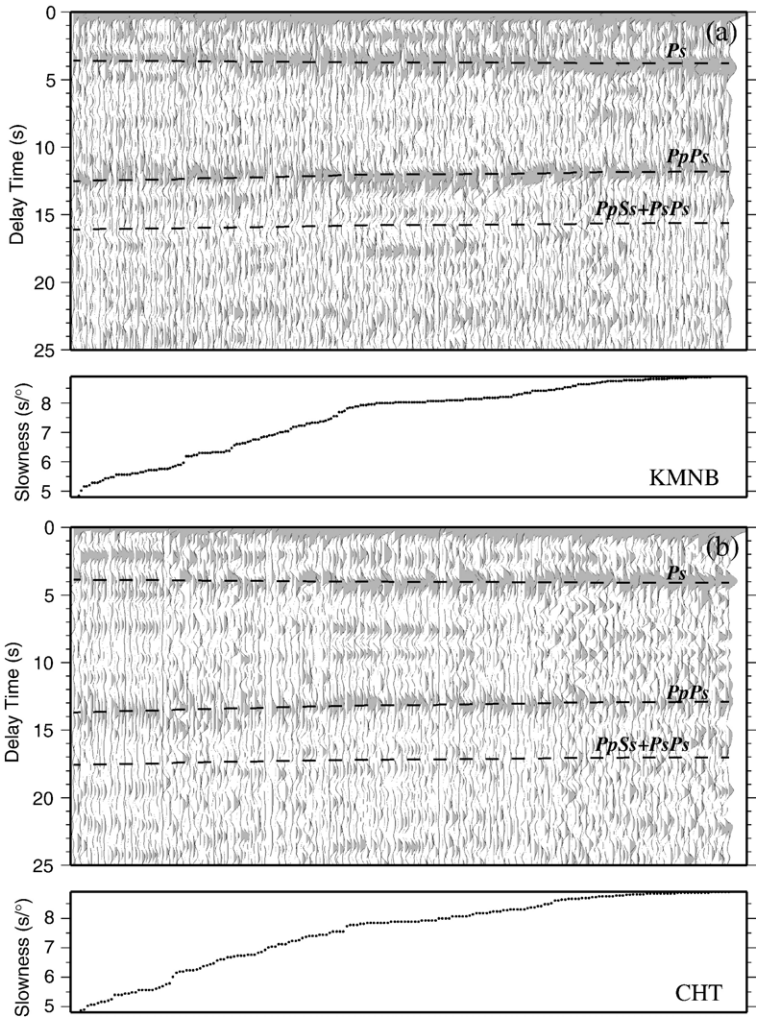

Fig. 3. Receiver function profiles for stations KMNB (shown only pasts of data for this station) in a and CHT in b, sorted according to slowness. The dashed lines show the predicted arrival times of Moho converted and reflected waves using the crustal parameters in Fig. 4a and c, respectively.

Fig. 3 shows two selected profiles of receiver functions recorded by stations KMNB and CHT. We can identify strong converted phases from the Moho at around 3.5 s and also clearly identify PpPs for both of them. Station KMNB (Fig. 3a) belongs to the BATS array. Stacking its 340 receiver functions gives a crustal thickness of 29.1 km and a crustal V_P/V_S ratio of 1.77 (Fig. 4a). Station CHT (Fig. 3b) belongs to the FJN array. Stacking its 193 receiver functions gives a crustal thickness of 32.1 km and a crustal V_P/V_S ratio of 1.74 (Fig. 4c). The dashed lines correspond to the average travel time curves of the Moho converted and multiply reflected phases (Fig. 3).

Different networks showed very different H–k stacking results. As shown in supplementary Table 1 in the Appendix, we were able to estimate crustal thicknesses and V_P/V_S ratios for all 30 stations in mainland China, but only 4 of the 13 BATS stations. This discrimination is attributed to complicated site effect, large background noise, or contaminations from multiple phases at shallower discontinuities for BATS stations. H–k stacking results at 32 stations around the Fujian Province (stations KMNB and MATB are located in this region) show that the crustal thicknesses range from 28.3 to 32.8 km with an average value of 31.1 km; the V_P/V_S ratios vary from 1.70 to 1.84 with an average value of 1.76. The latter corresponds to Poisson's ratios from 0.236 to 0.291, with an average value of 0.259. On the island of Taiwan, we only obtained estimates for two stations. The crustal thicknesses and V_P/V_S ratios are 34.2 and 1.79 for station NACB, and 34.5 and 1.68 for station TWKB.

As examples of the stacking results, the stacking amplitude images of four stations are shown in Fig. 4. Station KMNB is a BATS station on the offshore of mainland China. The best estimation resulted from stacking its 340 receiver functions, leading to a crustal thickness of 29.1 km and a crustal V_P/V_S ratio of 1.77 (Poisson's ratio of 0.265) (Fig. 4a). For station NACB on Taiwan island, stacking its 244 receiver functions gives the best estimation of crustal thickness of 34.2 km with a crustal V_P/V_S ratio of 1.79 (Poisson's ratio of 0.272) (Fig. 4b). In the same way, for the FJN stations CHT and XIM, stacking 193 and 151 receiver functions results in crustal thicknesses of 32.1 and 29.6 km and crustal V_P/V_S ratios of 1.74 and 1.75 (Poisson's ratios 0.255 and 0.259), respectively (Fig. 4c,d). The distance between station XIM in the FJN array and station KMNB in the BATS array is small (Table 1 in the Appendix), the results obtained from H–k stacking for both stations are consistent with each other as expected.

Fig. 5 shows the crustal thicknesses and Poisson's ratios distributions in southeastern China constrained by H–k stacking. Because there are only two estimates of crustal thickness for Taiwan, crustal thickness contour

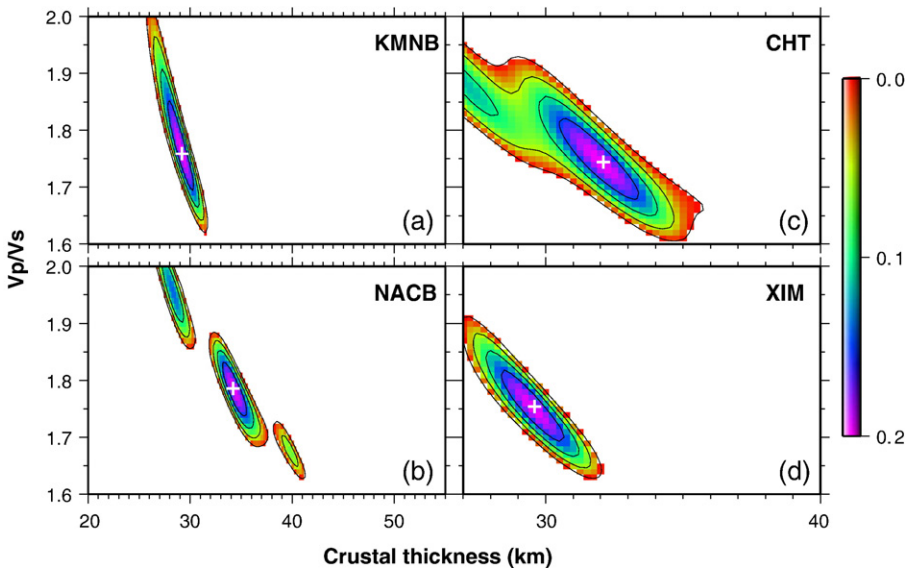

Fig. 4. H–k stacking results for V_P/V_S and crustal thicknesses under four seismic stations. The station codes are shown in the upper right corner. The different colors show the different stacking values, which cross symbols denote the best estimations when the correct crustal thicknesses and V_P/V_S ratios are used in the stacking.

lines are drawn without using this part of the data (Fig. 5). Our results indicate that the crustal thicknesses in the Fujian Province thin from west to east, and also thin from north to south. This crustal thickness variation is consistent with previous results obtained from other geophysical surveys (Chen et al., 2005; Li et al., 2006). The variation of Poisson's ratios is also shown for the Fujian Province. The Poisson's ratio increases from the west to offshore of the Fujian Province (Fig. 5).

4. CCP stacking results

4.1. The crustal and the uppermost mantle structure

In this study, two parallel CCP stacking profiles across the southeastern China region were selected (Fig. 1). They are oriented N125° E and were selected for the following reasons. A recent GPS study showed that the relative plate motion between the Eurasian plate and the Philippine Sea plate is directed N54° W at an estimated rate of 8.2 cm/yr (Yu et al., 1997). The *H–k* stacking results demonstrated that crustal thicknesses and V_P/V_S ratios vary similarly along this trend in the Fujian Province. These two profiles are nearly perpendicular to the tectonic faults of both Taiwan and Fujian (Fig. 1), and in some instances, the interaction between the Eurasian plate and the Philippine Sea plate can be shown in the same profiles.

Since the CCP stacking results are sensitive to the velocity structure, we used the 1D *iasp91* (Kennett and Engdahl, 1991) velocity model with a modified crustal structure for each station to convert each receiver function from the time-domain to the depth-domain. For stations near the Fujian Province (including stations KMNB and MATB in the BATS array), the *H–k* stacking results for crustal thicknesses and V_P/V_S ratios were used, instead of the 1D *iasp91* crustal model. For stations in Taiwan, the crustal models derived from previous tomographic velocity models were used, instead of the 1D *iasp91* crustal model (Ma et al., 1996). To

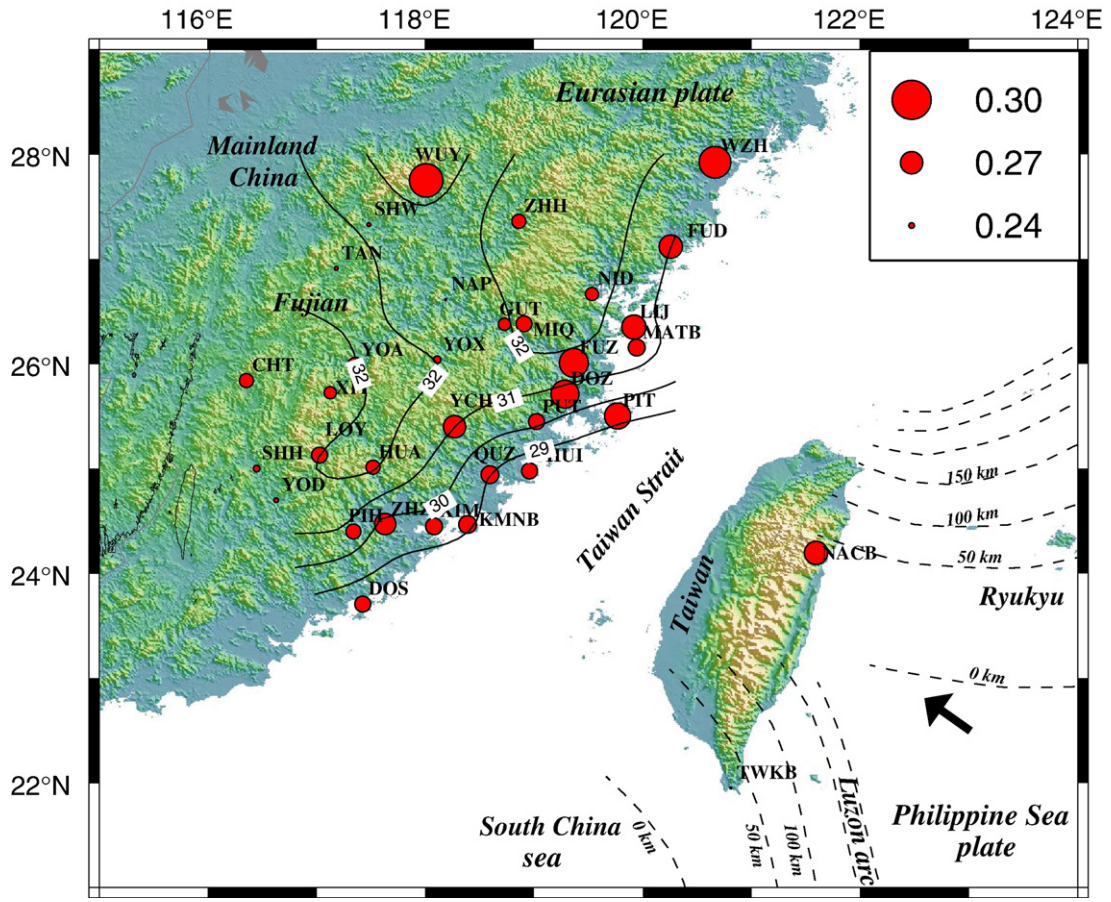

Fig. 5. The estimated crustal thicknesses and Poisson's ratios for 32 stations beneath Fujian and Taiwan. The contours of the crustal thickness are based on the data of 32 stations near Fujian. Station codes are shown near stations with three or four capital letters.

suppress high-frequency noise in the receiver functions, a second-order, zero phase, Butterworth bandpass filter with corner frequencies 0.03–1.0 Hz, was applied to all 5344 receiver functions. Due to the azimuthal dependence of radial receiver functions and more complicated structure in the uppermost mantle, we stacked receiver functions coming from a fixed range of azimuths. For profiles AA′ and BB′, we stacked receiver functions whose back-azimuths are in the bands from 80–170° to 260–350°. Finally, the CCP stacking was done along 2-D profiles. The width of the profiles is 200 km. In this way, the two profiles are completely separated from each other. A bin size of 4 km along the profile and 0.5 km in depth was used. The width of the ray along the profile was calculated by considering its Fresnel zone (Zhu, 2002). We applied a Gaussian window to smooth the stacking result, and the smoothing weight for each receiver function depended on the distance to the center of the bin. In this case, at a depth of 30 km, the bin size is a cuboid with 200 km in width, about 20 km along the profile, 0.5 km in thickness, respectively. All receiver functions with piercing points at depth of 30 km within this cuboid are stacked together to produce the smooth image.

The main results of the CCP stacking analyses for profiles AA′ and BB′ are shown in Fig. 6. The trends of both profiles AA′ and BB′ are nearly parallel to the subducting direction of the Philippine Sea plate. Both stacking profiles show about 600-km-long images of the upper mantle structure to a depth of 150 km. To evaluate the quality of the stacking images, at the top of each figure (Fig. 6a,b), the number of ray hits in each bin at a depth of 30 km was listed. For profile AA′, the number of ray hits ranges from 5 to 313 with an average value of 91 between longitude 116.2° and 118.7° in the Fujian area, and ranges from 8 to 155 with an average value of 62 between longitude 120.4° and 121.9° in the Taiwan region (Fig. 6a). In the same way for the profile BB′, the

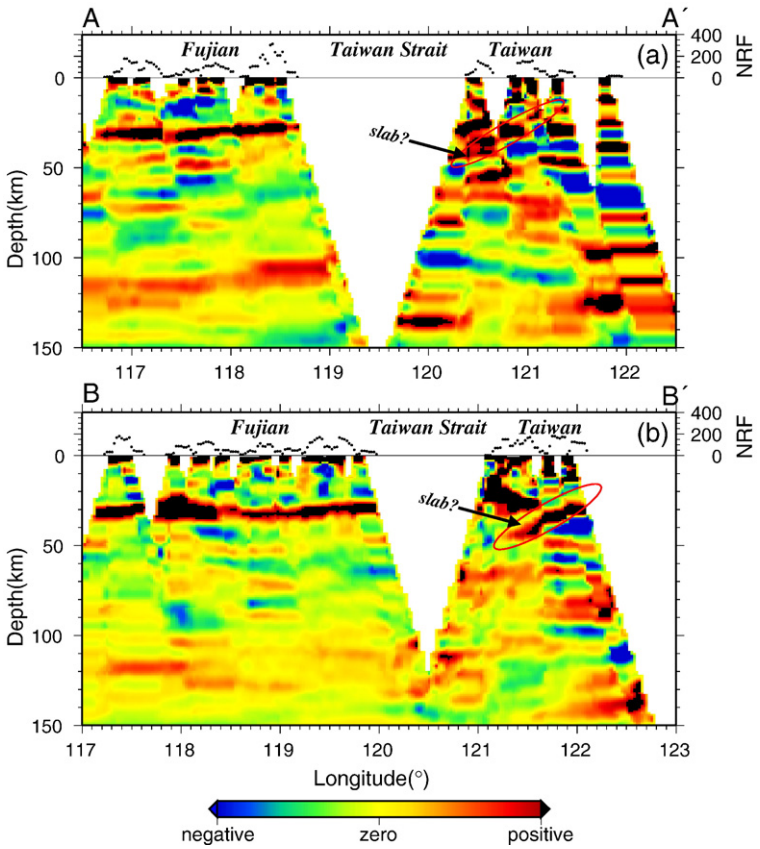

Fig. 6. CCP stacking of receiver function for lines AA′ (a) and BB′ (b) down to the depth of 150 km. Red (black) and blue colors denote the positive and negative stacking amplitude, respectively. Receiver functions, which back-azimuths are in the bands of 80–170° and 260–350° with bandpass filter 0.03–1.0 Hz, and a bin size of 4 km along the profile and 0.5 km in depth, are used in the CCP stacking for lines AA′ and BB′. NRF denote the number of receiver functions at depth of 30 km in each bin. Slabs images deduced by CCP stacking are shown with red ellipses.

number of ray hits ranges from 8 to 180 with an average value of 71 between longitude 117.2° and 120.0° in the Fujian area, and ranges from 4 to 181 with an average value of 99 between longitude 121.1° and 122.1° in the Taiwan region (Fig. 6b). In the Fujian region, both stacking profiles show a consistent Moho with strong converted phases at depths around 30 km (Fig. 6a,b). From NW to SE, the depths of the Moho for both profiles turn shallow from 32 km to 29 km. On the other hand, in Taiwan, the CCP stacking results show more complicated images from the surface to a depth of 50 km. Because of the interaction between the Eurasian plate and the Philippine Sea plate in this region, Moho phases have a much more complicated structure. In Fig. 6a, between longitude 120.3° and 121.8°, and at depths of 25–30 km, there can be seen a strong converted phase which may represent the Moho. However, between longitude 120.4° and 121.3°, and at depths of 45–15 km, a possible NW dipping converted phase can be seen, marked by an ellipse, which is stacking noise or the top of Philippine Sea plate (Fig. 6a). In the same way, in Fig. 6b, between longitude 120.1° and 120.6°, and at depths of 20–30 km, a possible Moho image can be seen. However, between longitude 121.2° and 122.1° and at depths of 30–50 km, a strong NW dipping clear converted phase marked by an ellipse is imaged, which is interpreted as the possible top of Philippine Sea plate (Fig. 6b, see Discussion section in detail).

4.2. The upper mantle discontinuities

We also used the CCP stacking of receiver functions to study the upper mantle discontinuities beneath southeast China along the above two profiles. The method and parameters used for these profiles are the same as in the study of the crust and uppermost mantle structure with a few differences. Firstly, in this section, all 5344 receiver functions were used to constrain the 410 and the 660 structure along the two stacking profiles. Secondly, to suppress high-frequencies noise contamination in the deep structure, a second-order, zero phase, Butterworth bandpass filter with corner frequencies 0.03–0.2 Hz was applied to all receiver functions before the CCP stacking was carried out. Finally,

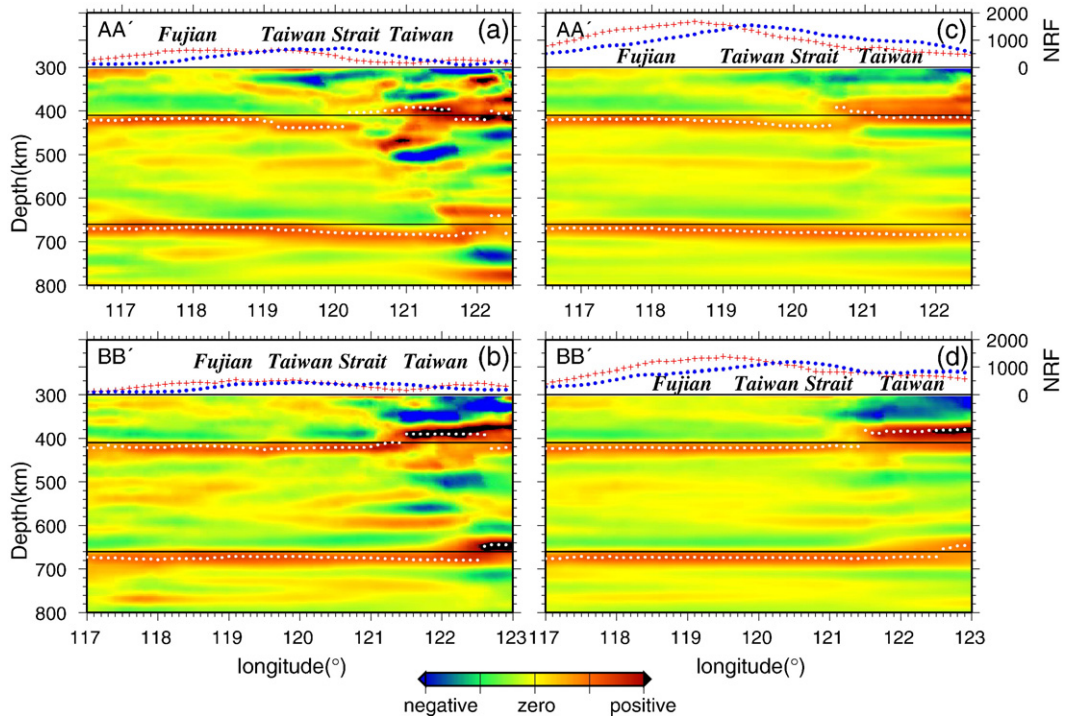

Fig. 7. CCP stacking of receiver function for profiles AA′ (a), BB′ (b) with smaller smoothing parameters, AA′ (c) and BB′ (d) with larger smoothing parameters between the depths of 300 and 800 km. The 410- and the 660-km discontinuities are clearly imaged with simple and flat feature beneath Fujian and Taiwan Strait. Positive polarity energy is plotted in red color. Red cross and blue dot denote the number of receiver functions (NRF) in each bin at depths of 410 km and 660 km, respectively. The observed depths of discontinuities are denoted with white dots. The depth domain images are calculated from 1D *iasp91* velocity model with a modified crustal structure for each station.

two different types of smoothing parameters (different Fresnel zone sizes and widths) were considered. When the smaller smoothing parameters were used, the widths of bins are 100 km, at depths of 410 km and 660 km, the lengths of bins along the profile are about 130 km (~65 km in radius) and 200 km (~100 km in radius), respectively (Fig. 7a,b). In the same way, when the larger smoothing parameters were used, the widths of bins are 150 km, at depths of 410 km and 660 km, the lengths of bins along the profile are about 260 km (~130 km in

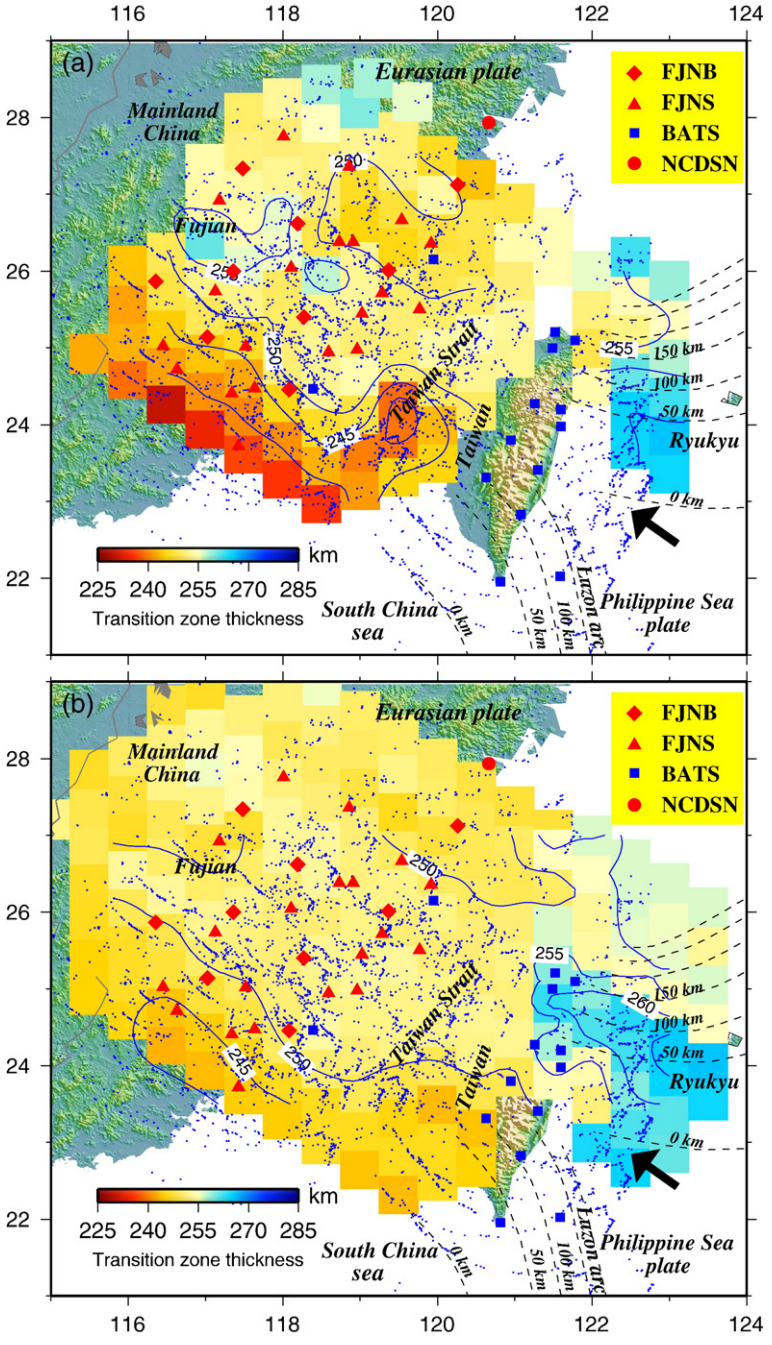

Fig. 8. Transition zone thickness (TZT) variations in the study region. The TZT is determined by subtracting the depth of the 660 from that of the 410 for each bin in the study profile. Contours lines denote the transitional zone thickness variations. See captions in Fig. 1 for more interpretation.

radius) and 400 km (~200 km in radius), respectively (Fig. 7c,d).

The CCP stacking results are illustrated in Fig. 7. The results in the transition zone cover the entire study region due to the ray-paths crossing each other, even across the Taiwan Strait. At the top of each figure (Fig. 7a,b,c,d), the number of ray hits in each bin were listed at depths of 410 km and 660 km with crosses and dots, respectively. For different smoothing parameters, the number of ray hits changes largely for the same stacking profile. For the profile AA′, the number of ray hits ranges from 122 to 638 with an average value of 399 at a depth of 410 km, and ranges from 92 to 702 with an average value of 365 at a depth of 660 km when the smaller smoothing parameters are used (Fig. 7a). However, the number of ray hits ranges from 444 to 1678 with an average value of 1058 at a depth of 410 km, and ranges from 511 to 1541 with an average value of 1033 at a depth of 660 km when the larger smoothing parameters are used (Fig. 7c). For different smoothing parameters, the 410 and the 660 almost remain unchangeable except in the east part of the profiles. Beneath the Fujian and Taiwan Strait, the 410 and the 660 (maximum amplitude part of converted phase shown in Fig. 7 with a white dotted line) are shown as flat and continuous positive phases clearly (Fig 7a,b, c,d). The depths of the 410 are about 420 km, and the depths of the 660 are around 670 km, except to the east and the southeast of Taiwan. However, beneath the east of Taiwan island, the 410 cannot be clearly traced at longitudes between 120.5° and 122.5° for profile AA′, and at longitudes between 121.3° and 123.0° for profile BB′ (Fig. 7a,b). In this region, almost all stacking data from stations on the Taiwan island, the depths of the 410 and the 660 are uplifted in the same manner, which may indicate unsuitable velocity models used on the Taiwan island or due to multiple phase contamination from shallow discontinuity structure. An image of the 520 km discontinuity cannot be seen in any stacking profile, which is interpreted as the phase transformation from β-spinel to γ-spinel of olivine (Shearer, 1990).

In this study, due to the absence of a detailed three-dimensional P and S wave velocity structure in southeast China, we converted receiver functions from the time domain to the depth domain only using the 1D *iasp91* velocity model with a modified crustal structure in this region. Therefore, the absolute depths of the upper mantle discontinuities probably have some bias and should be considered with caution. However, it is considered that the mantle transition zone (TZT) has a relatively small heterogeneous structure compared with that of the upper mantle down to about 410 km depth (Bostock, 1996; Vinnik et al., 1996). Hence, we focus our study on the TZT variation rather than the absolute depths of the upper mantle discontinuities. In order to avoid the influence of different velocity models, all data were grouped into two parts which ones are from stations on Fujian (including stations KMNB and MATB) and the others are from station on the Taiwan island. Two parts of data were stacked separately along the same stacking profile. Thirteen lines parallel to profile AA′ were selected and CCP stacking was performed along each profile by using different smoothing parameters. Two adjacent profiles have a spacing of 0.5° latitude interval and the CCP stacking covers almost the entire study region.

In order to investigate the TZT variation in the study region, we determined the depths corresponding to the maximum positive amplitude of the 410 and the 660 in the bands of 380–440 km and 640–680 km in each bin along the stacking profiles. The TZT was calculated by subtracting the depth of the 660 from that of the 410 for each point. During the calculation, we only selected bins with over 100 receiver functions for analysis. As shown in Fig. 8, the change in TZT varies within ±5 km from 250 km in the Fujian Province and Taiwan Strait even though different smoothing parameters were used (Fig. 8a,b). However, in the east of Taiwan, TZT variations thicken from west to east, with the thickest part about 265 km (Fig. 8a,b).

5. Discussion

5.1. Crustal thickness and Poisson's ratio variations in Fujian

A general increasing trend in Poisson's ratio from inland to offshore of the Fujian Province may indicate different crustal composition. Geologically, the Late Mesozoic igneous rocks spread widely across a zone parallel to the coastline of the Fujian Province, and they include Early Yanshanian rocks (180–140 Ma) distributed on the landward region and Late Yanshanian rocks (140–97 Ma) distributed on the oceanward region (Zhou and Li, 2000). The amount of volcanic rocks increases oceanward. Most felsic rocks appear to be more widespread in the coastal area in Fujian, and chemically, they are mainly calc-alkaline and high-K calc-alkaline series. On the other hand, large peraluminous granitoids exist widely in the inland area of the Fujian Province, and are chemically high in SiO_2 and Na_2O (Zhou and Li, 2000). From mineral experiment, we know that, for common plutonic igneous rocks, there is a clear trend between Poisson's ratio and composition (Christensen, 1996). A

linear correlation of decreasing Poisson's ratio with increasing SiO_2 is observed for granitoids. Moreover, a correlation of increasing Poisson's ratio with increase in the anorthite content of plagioclase feldspar is found (Christensen, 1996). Therefore, the higher Poisson's ratios for coastal stations may be attributed to decreasing SiO_2 and increasing calc-alkaline contents in the crust.

The crustal thickness from this study is consistent with previous geophysical studies in the Fujian Province. Inversion of the Bouguer gravity anomaly demonstrates that crustal thickness tends to thin from inland to the coastal region in Fujian (Chen et al., 2005). Furthermore, exploration seismology also yields the same results (Liao et al., 1988). The same trend in crustal thickness in Fujian from different geophysical data indicates that crustal thinning near the coastal region is a robust feature. The crustal thinning in the coastal area of Fujian may be attributed to the following factors. First, this region is located in the transition zone from continental to oceanic crust, therefore, crustal thickness thins from inland to the coastal area. Second, due to the collision between the Eurasian plate and the Philippine Sea plate, the extent of the South China Sea turns wide, with a crustal thickness of the only about 10–15 km near its center from geophysical survey (Ma, 1989).

5.2. Crustal thickness and Poisson's ratio variations in Taiwan

Taiwan is located on the convergent boundary of two collision plates. Thus, mountain building processes and tectonic evolution in Taiwan are very complex. Unfortunately, we only obtained *H–k* results from two stations (NACB, TWKB) in Taiwan. These results are too sparse to constrain the crustal thicknesses and Poisson's ratios over the entire island. Station TWKB is located at the southern tip of the island. The crustal thickness obtained by using receiver functions is about 30–32 km by assuming an averaged V_P/V_S of 1.73 beneath this station (Kim et al., 2004). In the *H–k* stacking scheme, the crustal thickness tends to be larger with decreasing V_P/V_S ratio (Zhu and Kanamori, 2000). Therefore, the study's results for crustal thickness of 34.5 km and V_P/V_S of 1.68, are consistent with a previous study (Kim et al., 2004). On the contrary, the crustal thickness obtained by the *H–k* stacking scheme for station NACB is largely inconsistent with previous results (Yeh et al., 1998; Kim et al., 2004). The crustal thickness of about 45 km was obtained from wide-angle deep seismic profiling near the station NACB (Yeh et al., 1998). On the other hand, a crustal thickness of 50 km was also obtained by using receiver function analysis (Kim et al., 2004). But in this study, a crustal thickness of 34 km was obtained beneath the same station. This difference might be due to misidentification of the Moho and slab phases by different methods. To investigate these discrepancies, we have checked all our receiver functions and *H–k* results carefully for this station and have confirmed our results (Fig. 4b and supplement Fig. 1 in the Appendix). However, the station NACB is located near the most active and complex collision area in Taiwan (Kim et al., 2004), where more geophysical data and other pieces of evidence are required to get definite measurements of the crustal thickness.

5.3. Slab images

The existence of a subducting lithosphere slab beneath central Taiwan is important for a better understanding of the tectonic evolution of Taiwan. This question has remained unanswered (Chen et al., 2004). The observations of seismic waveforms and travel times for central Taiwan stations suggested that an eastern dipping aseismic slab may exist beneath central Taiwan (Chen et al., 2004). Based on the East Asia plate kinematic reconstructions, the geometry of plate boundaries, as well as the character of the deformation in Taiwan, Sibuet and Hsu (2004) suggested the following consequences of a geodynamic model in central Taiwan. A tear fault within the Eurasian continent beneath central Taiwan was created by the westward motion of the Philippine Sea plate. Then, the Eurasian continent was torn into two parts. One is the deeply subducting Eurasian continent slab underlying the Philippine Sea plate from central to southern Taiwan. The other is the upper Eurasian plate with the boundary of the Ryukyu forearc in northern Taiwan (Sibuet and Hsu, 2004). The mechanism of the Taiwan uplift is presumed to be produced by the slab pull force due to the Eurasian continent subduction (Sibuet and Hsu, 2004). Derived from an array analysis of long-period surface waves in Taiwan, a crustal thicknesses of about 40–45 km and relatively low velocities as well as a similar thickness of lithosphere to that of the adjacent sea area of mainland China, have been obtained beneath central Taiwan (Hwang and Yu, 2005). These results support the previous assumptions that a mountain root and an eastern dipping Eurasian slab may exist beneath central Taiwan (Rau and Wu, 1995; Chen et al., 2004).

However, our results show a different collision structure between the Eurasian continental slab and the

Philippine Sea plate near central and northern Taiwan (Fig. 6b). From the stacking results in Fig. 6a and b, we suggest that a western dipping Philippine Sea plate, rather than an eastern dipping Eurasian slab, possibly exists beneath central and northern Taiwan. This sugestion is strengthened by the following pieces of evidence. 1) Compared with the cold dense oceanic lithosphere, the continental lithosphere resists subduction due to its thick crust and buoyancy (Davies and von Blanckenburg, 1995). Therefore, the subduction of the Philippine Sea plate beneath the Eurasian continental slab is possible. 2) The relative motion between the Eurasian continental slab and the Philippine Sea plate is in the direction of NW, with an estimated rate of 8.2 cm/yr near central and northern Taiwan (Yu et al., 1997). The subduction of the Philippine Sea plate beneath central and northern Taiwan can explain this motion. However, if our slab images near central and northern Taiwan are true, several questions should be considered. Firstly, if the Philippine Sea plate is subducting to more than 200 km depth beneath the Eurasian continental along the Ryukyu forearc in northeastern Taiwan, why does it have a shallow feature in central and northern Taiwan? Secondly, why are there no intermediate-depth earthquakes beneath this region? The possible reasons might be, first, that subducting Philippine Sea plate terminates at central Taiwan with westward motion, rather than at northeastern Taiwan. Strong resistive forces from the Eurasian continental slab may make the collision region hot and ductile. Second, the lower part of the Philippine Sea plate is detached at a depth of about 50 km beneath central and northern Taiwan, but, is subducting to large depths beneath northeastern Taiwan. Because of the sparse data used in the CCP stacking, stacking noise and multiples from shallow structure, or Moho offset also could make the stacking results biased. Therefore, more extensive coverage of seismic stations or other geophysical data and extraordinary efforts should be considered in the future to confirm our interpretations.

5.4. The upper mantle discontinuities and TZT variations

Located on the western Pacific margin, southeast China provides an ideal region to study the dynamics of the upper mantle from the detailed analysis of the 410 and the 660 structure. Beneath Fujian and Taiwan Strait, the 410 and the 660 show a sharp and continuous feature (Fig. 7). Mineral physics studies suggest that the 410 may be shallower and the 660 may be deeper, and the 660 may present a complex feature in the subduction region (Ito and Takahashi, 1989; Vacher et al., 1998). However, our results in Fig. 7 do not show this to be the case. Except for east of Taiwan in Fig. 7(a, c) and Fig. 7 (b, d), the 410 shows a sharp and flat feature beneath Fujian and Taiwan Strait even though different smoothing parameters are used, and the depths of the 410 are about 420 km. Furthermore, the 660 shows a simple structure with only one strong positive phase at a depth of around 670 km. We do not find a complex 660 structure which was found in other subduction regions (Simmons and Gurrola, 2000; Ai et al., 2003). Therefore, from the structure of both the 410 and the 660, our study suggests that the upper mantle discontinuities beneath Fujian and Taiwan Strait are less affected by subduction. However, in the east of Taiwan in Fig. 7(a) and Fig. 7(b), the 410 and the 660 show a complex feature and tend to be shallower. The complex structure of the 410 and the 660 beneath the east of Taiwan may be attributed as follows. When the improper velocity models in Fujian or Taiwan are used in the transformation from time-domain to depth-domain, the depths of 410 and 660 could be calculated with bias due to ray-paths crossing from different regions. Secondly, the stacking phases of 410 and 660 could be influenced by multiple phases from shallower discontinuities.

Variations in the TZT can supply more information about the temperature change in the transition zone than the absolute depths of the 410 and the 660 (Owens et al., 2000). Compared with the global average of 250 km for the TZT, the results for the TZT anomalies remain within ±5 km beneath Fujian and Taiwan Strait (Fig. 8a, b). Furthermore, TZT results from the global *SS* stacking, which uses long-period *SS* precursors from underside reflections off upper mantle discontinuities, show about 250 to 260 km beneath this region (Flanagan and Shearer, 1998; Gu and Dziewonski, 2002). A recent tomographic study beneath south Taiwan revealed a high-velocity zone from the surface down to a depth of 300 km (Wang et al., 2006). These results suggest that the temperature of the transition zone in this region is almost the same as that of ambient mantle. Therefore, the TZT anomalies from this study support the suggestion that the transition zone beneath Fujian and Taiwan Strait is less affected by the Eurasian plate, and if the Eurasian subducting slab exists beneath this region, it should be confined to a depth above 410 km. On the other hand, at the east longitude 122.0° of Taiwan, the TZT is about 260 to 265 km (Fig. 8a,b). This study is consistent with previous tomographic results, which suggested the South China Sea slab reaching the transition zone beneath this region (Lallemand et al., 2001).

6. Conclusions

Based on the detailed analyses of receiver functions from 44 stations beneath Fujian and Taiwan, the main conclusions of this study are as follows:

(1) Crustal thickness and Poisson's ratio
Near the Fujian Province, results from H–k stacking at 32 stations demonstrate that the crustal thicknesses range from 28.3 to 32.8 km with an average value of 31.1 km, and the V_P/V_S ratios vary from 1.70 to 1.84 with an average value of 1.76, which correspond to Poisson's ratios from 0.236 to 0.291 with an average value of 0.259. The crustal thicknesses tend to thin and Poisson's ratios tend to increase from inland to offshore of the Fujian Province, which may indicate a decrease in SiO_2 and increase in calc-alkaline content in the crust beneath offshore stations. However, due to the complex mountain building processes and tectonic evolution, the study cannot confine the crustal thicknesses and Poisson's ratios well in Taiwan by the *H–k* stacking method.

(2) Slab configuration
In central and northern Taiwan, the CCP stacking of receiver functions shows a western dipping positive phase down to the depth of 50 km. This result leads to the suggestion that the Philippine Sea plate is probably subducting beneath Eurasian continent plate near central and northern Taiwan. However, due to sparse data and tectonic complexity on Taiwan, this suggestion will need further work with more data.

(3) The upper mantle discontinuities and transition zone thickness.
The 410 and the 660 show a sharp and continuous feature by using CCP stacking of receiver functions beneath Fujian and Taiwan Strait. The TZT and the temperature of the transition zone are almost the same as that of ambient mantle in the most studied region. Both the upper mantle discontinuities and TZT structures, support the conclusion that the transition zone beneath Fujian and Taiwan Strait is less affected by the Eurasian plate, and if such a subduction exists, it should be confined to a depth above 410 km. In contrast, the South China Sea slab may reach the transitional zone in the east of Taiwan due to thickening TZT there.

Acknowledgments

We thank Qingju Wu, Lupei Zhu, and Weiwei Xu for providing parts of their codes, Stephen Hartzell, Chen Ji, and Pengcheng Liu for proofreading the manuscript. Constructive reviews were provided by Rob D. van der Hilst and two anonymous reviewers for their helpful comments. All the waveforms of BATS and TATO stations were provided by IES, Academic Sinica, Taiwan through the IRIS Data Management Center. The GMT software package distributed by Wessel and Smith (Wessel and Smith, 1995) was used for plotting the figures. This research was supported by grants from National Natural Science Foundation of China (NSFC grants 40474022 and 40674020).

Appendix A. Supplementary data

Supplementary data associated with this article can be found, in the online version, at doi:10.1016/j.epsl.2007.06.009.

References

Ai, Y., Zheng, T., Xu, W., He, Y., Dong, D., 2003. A complex 660 km discontinuity beneath northeast China. Earth Planet. Sci. Lett. 212, 63–71.

Ai, Y., Zhao, D., Gao, X., Xu, W., 2005. The crust and upper mantle discontinuity structure beneath Alaska inferred from receiver funcions. Phys. Earth Planet. Inter. 150, 339–350.

Ammon, C.J., 1991. The isolation of receiver function effects from teleseismic P waveforms. Bull. Seismol. Soc. Am. 81, 2504–2510.

Bostock, M.G., 1996. Ps conversions from the upper mantle transition zone beneath the Canadian landmass. J. Geophys. Res. 101, 8393–8402.

Chen, P.F., Huang, B.S., Liang, W.T., 2004. Evidence of a slab of subducted lithosphere beneath central Taiwan from seismic waveforms and travel times. Earth Planet. Sci. Lett. 229, 61–71.

Chen, X., Lin, S., Li, Z., Bao, T., Zhou, Z., 2005. Preliminary 1D model for crust velocity structure in Fujian–Taiwan region. Earthquake 25, 61–68.

Chevrot, S., van der Hilst, R.D., 2000. The Poisson ratio of the Australian crust: geological and geophysical implications. Earth Planet. Sci. Lett. 183, 121–132.

Christensen, N.I., 1996. Poisson's ratio and crustal seismology. J. Geophys. Res. 101, 3139–3156.

Davies, J.H., von Blanckenburg, F., 1995. Slab breakoff: a model of lithosphere detachment and its test in the magmatism and deformation of collisional orogens. Earth Planet. Sci. Lett. 129, 85–102.

Dueker, K.G., Sheehan, A.F., 1997. Mantle discontinuity structure from midpoint stacks of converted P to S waves across the Yellowstone hotspot track. J. Geophys. Res. 102, 8313–8327.

Flanagan, M.P., Shearer, P.M., 1998. Global mapping of topography on transition velocity discontinuities by stacking SS precursors. J. Geophys. Res. 103, 2673–2692.

Font, Y., Lallemand, S., Angelier, J., 1999. Etude de la transition entre l'orogène actif de Taiwan et la subduction des Ryukyu-Apport de la sismicité. Bull. Soc. Géol. Fr. 170, 271–283.

Gu, Y.J., Dziewonski, A.M., 2002. Global variability of transition zone thickness. J. Geophys. Res. 107. doi:10.1029/2001JB000489.

Gudmundsson, O., Sambridge, M., 1998. A regionalized upper mantle (RUM) seismic model. J. Geophys. Res. 103, 7121–7136.

Hwang, R.D., Yu, G.K., 2005. Shear-wave velocity structure of upper mantle under Taiwan from the array analysis of surface waves. Geophys. Res. Lett. 32, L07310. doi:10.1029/2004GL021868.

Ito, E., Takahashi, E., 1989. Postspinel transformations in the system Mg_2SiO_4–Fe_2SiO_4 and some geophysical implications. J. Geophys. Res. 94, 10637–10646.

Kao, H., Jian, P.R., Ma, K.F., Huang, B.S., Liu, C.C., 1998. Moment tensor inversion for offshore earthquakes east of Taiwan and their implications to regional collision. Geophys. Res. Lett. 25, 3619–3622.

Kennett, B.L.N., Engdahl, E.R., 1991. Traveltimes for global earthquake location and phase identification. Geophys. J. Int. 105, 429–465.

Kim, K.H., Chiu, J.M., Kao, H., Liu, Q., Yeh, Y.H., 2004. A preliminary study of crustal structure in Taiwan region using receiver function analysis. Geophys. J. Int. 159, 146–164.

Kosarev, G., Kind, R., Sobolev, S.V., Yuan, X., Hanka, W., Oreshin, W., 1999. Seismic evidence for a detached Indian lithospheric mantle beneath Tibet. Science 283, 1306–1309.

Lallemand, S., Font, Y., Bijwaard, H., Kao, H., 2001. New insights on 3-D plates interaction near Taiwan from tomography and tectonic implications. Tectonophysics 335, 229–253.

Langston, C.A., 1977. The effect of planar dipping structure on source and receiver responses for constant ray parameter. Bull. Seismol. Soc. Am. 67, 1029–1050.

Li, S., Mooney, W.D., Fan, J., 2006. Crustal structure of mainland China from deep seismic sounding data. Tectonophysics 420, 239–252.

Liao, Q., Wang, Z., Wang, L., Yu, Z., Wu, N., Liu, B., 1988. Explosion seismic study of the crustal structure in Fuzhou–Quanzhou–Shantou region. Chin. J. Geophys. 31, 270–280 (in Chinese with English abstract).

Ma, X., 1989. Lithospheric Dynamic Atlas of China. China Cartographic Publishing House, Beijing. 39–40 pp., (in Chinese with English abstract).

Ma, K.F., Wang, J.H., Zhao, D., 1996. Three-dimensional seismic velocity structure of the crust and uppermost mantle beneath Taiwan. J. Phys. Earth 44, 85–105.

Owens, T.J., Nyblade, A.A., Gurrola, H., Langston, C.A., 2000. Mantle transition zone structure beneath Tanzania. Geophys. Res. Lett. 27, 827–830.

Rau, R.J., Wu, F.T., 1995. Tomographic imaging of lithospheric structures under Taiwan. Earth Planet. Sci. Lett. 133, 517–532.

Shearer, P.M., 1990. Seismic imaging of upper mantle structure with new evidence for a 520-km discontinuity. Nature 344, 121–126.

Sibuet, J.C., Hsu, S.K., 2004. How was Taiwan created? Tectonophysics 379, 159–181.

Simmons, N.A., Gurrola, H., 2000. Multiple seismic discontinuities near the base of the transition zone in the Earth's mantle. Nature 405, 559–562.

Suppe, J., 1984. Kinematics of arc–continent collision, flipping of subduction, and back-arc spreading near Taiwan. Mem. Geol. Soc. China 6, 21–34.

Vacher, P., Mocquet, A., Sotin, C., 1998. Computation of seismic profiles from mineral physics: the importance of the nonolivine components for explaining the 660 km depth discontinuity. Phys. Earth Planet. Inter. 106, 275–298.

Vinnik, L.P., 1977. Detection of waves converted from P to SV in the mantle. Phys. Earth Planet. Inter. 15, 39–45.

Vinnik, L.P., Kosarev, G., Petersen, N., 1996. Mantle transition zone beneath Eurasia. Geophys. Res. Lett. 23, 1485–1488.

Wang, Z., Zhao, D., Wang, J., Kao, H., 2006. Tomographic evidence for the Eurasian lithosphere subducting beneath south Taiwan. Geophys. Res. Lett. 33. doi:10.1029/2006GL027166.

Wessel, P., Smith, W.H.F., 1995. New version of the Generic Mapping Tools (GMT) version 3.0 released. EOS Trans. AGU 76, 329.

Wu, Q., Zeng, R., 1998. The crustal structure of Qinghai–Xizang plateau inferred from broadband teleseismic waveform. Chin. J. Geophys. 41, 669–679 (in Chinese with English abstract).

Wu, F.T., Rau, R.J., Salzberg, D., 1997. Taiwan orogeny: thin-skinned or lithospheric collision? Tectonophysics 274, 191–220.

Yeh, Y.H., Shih, R.C., Lin, C.H., Liu, C.C., Yen, H.Y., Huang, B.S., Liu, C.S., Chen, P.Z., Huang, C.S., Wu, C.J., Wu, F.T., 1998. Onshore/offshore wide-angle deep seismic profiling in Taiwan. TAO 9, 301–316.

Yu, S.B., Chen, H.Y., Kuo, L.C., 1997. Velocity field of GPS stations in the Taiwan area. Tectonophysics 274, 41–59.

Yuan, X., Ni, J., Kind, R., Mechie, J., Sandvol, E., 1997. Lithospheric and upper mantle structure of southern Tibet from a seismological passive source experiment. J. Geophys. Res. 102, 27491–27500.

Zandt, G., Ammon, C.J., 1995. Continental-crust composition constrained by measurements of crustal Poissons ratio. Nature 374, 152–154.

Zhou, X.M., Li, W.X., 2000. Origin of Late Mesozoic igneous rocks in Southeastern China: implications for lithosphere subduction and underplating of mafic magmas. Tectonophysics 326, 269–287.

Zhu, L., 2000. Crustal structure across the San Andreas Fault, Southern California from teleseismic converted waves. Earth Planet. Sci. Lett. 179, 183–190.

Zhu, L., 2002. Deformation in the lower crust and downward extent of the San Andreas Fault as revealed by teleseismic waveforms. Earth Planets Space 54, 1005–1010.

Zhu, L., Kanamori, H., 2000. Moho depth variation in southern California from teleseismic receiver functions. J. Geophys. Res. 105, 2969–2980.